AIRFRAME VIBRATION CONTROL SIMULATION OF A MEDIUM UTILITY HELICOPTER USING A HIGHER HARMONIC CONTROL SYSTEM

Do-Hyung Kim, Korea Aerospace Research Institute, Daejeon, Korea
Jae-Sang Park, Chungnam National University, Daejeon, Korea
Dong-Gyue Kim, Chungnam National University, Daejeon, Korea
Woo-Ram Kang, Korea Aerospace Industries, Sacheon, Korea

Abstract

A numerical simulation of the airframe vibration control of a medium utility helicopter using the higher harmonic control (HHC) system has been performed. The HHC system operates independently of the primary control system. For the aeromechanical analysis, CAMRAD II is used to model the target aircraft including the main rotor, tail rotor and airframe. The reliability of the analytical model predictions of the airframe vibration response characteristics is validated by comparison with flight test data. The helicopter model of the vibration control system is constructed by calculating the uncontrolled vibrations that occur in the level flight conditions and the vibrations generated by the HHC actuation, and then performing off-line system identification. Using the constructed system model, the optimal control to reduce the main rotor vibratory hub load is evaluated. Then the optimal control for airframe vibration reduction is investigated, and the control inputs and vibration characteristics of the optimal main rotor vibratory hub load reduction control and the optimal airframe vibration reduction control are compared and discussed. It is observed that at low-speed flight condition, a larger control input is required to reduce airframe vibration than to reduce the vibratory hub load and that the optimum control input for airframe vibration reduction does not reduce the F_z component of the vibratory hub load.

1. INTRODUCTION

Active rotor control has been extensively studied since the 1950s, mainly through higher harmonic control (HHC) systems (Refs. 1, 2). These systems consist of actuators located below the swashplate and introduce harmonics N_b - 1, N_b, N_b + 1/rev to the rotor blades by the actuator motion with an operating frequency of N_b/rev, where N_b is the number of blades. The HHC system considered in this study is installed between the main rotor actuator (MRA) and the nonrotating swashplate as shown in Figure 1, and the primary control by the pilot and the HHC system are operated independently. The two control inputs, primary control and HHC, are combined to produce the total blade pitch change. The HHC system has the advantage of having all components in a nonrotating frame in the fuselage, which can make safety and certification issues easy to clear. Early HHC systems

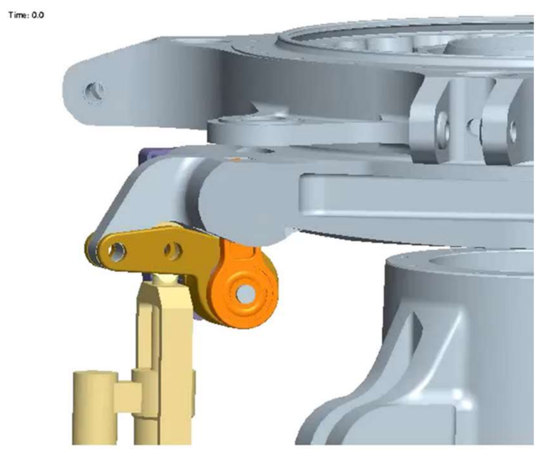

Figure 1: Example HHC actuator geometry (Rendering reproduced by courtesy of Airbus Helicopters Technik GmbH, compare Patents DE 10 2013 223 508 B4, B64C 27/605 (2006.01)).

utilized hydraulic actuators to demonstrate the HHC technology, which had the disadvantages of requiring large amounts of power and were heavy. However, recent advances in electro-mechanical actuator technology have made it possible to develop more feasible HHC systems using small electro-mechanical actuators.

In order to develop an HHC system, it is necessary to study the applicability to the target helicopter, the effects of the system and the required actuator control capability. The authors (Ref. 3) investigated the feasibility and effectiveness of the HHC system for a medium utility helicopter by numerical simulation. In this simulation, an isolated rotor model was constructed using CAMRAD II and the effectiveness of the HHC system in reducing N_b/rev vibratory hub loads was demonstrated. However, the ultimate goal of implementing the HHC system on a real helicopter is to eliminate airframe vibration. To evaluate the vibration reduction performance of the HHC system, it is essential to build a comprehensive analysis model that includes an elastic airframe. In addition, it is important to evaluate whether vibratory hub loads are also reduced when an HHC system is used to minimize airframe vibration. In this study, a CAMRAD II model including an elastic airframe for a medium utility helicopter is constructed and the optimal vibration control characteristics that minimize vibratory hub load and airframe vibration have been investigated. In addition, the effect of the optimal airframe vibration reduction control input on hub load changes and, conversely, the effect of the optimal vibratory hub load reduction control input on airframe vibration reduction were compared and discussed.

2. HELICOPTER MODEL

2.1. CAMRAD II modeling

The medium utility helicopter considered for the application of the HHC system in this study is a four-bladed (7.9 m radius) aircraft with a maximum take-off weight of 8,709 kg, a maximum cruise speed of 150 knots, and an operating altitude of 4,595 meters. The rotorcraft comprehensive analysis code, CAMRAD II, is used to simulate the helicopter model. In order to output the vibration response of the airframe, it is necessary to construct an entire helicopter model including main rotor, tail rotor and elastic airframe. The main rotor blade structure is discretized into 8 nonlinear beam finite elements and the rotor control system including swashplates, pitch-links and pitch-horns is modeled in a sophisticated way. The rotor aerodynamic model used is based on the ONERA EDLIN unsteady theory with C81 airfoil table lookup. For calculation of the main rotor aerodynamic loads, each blade is divided into 21 aerodynamic panels. A multiple-trailer wake model with consolidation is used to compute the non-uniform induced velocities around the rotor. The tail rotor is modeled in the same way. The elastic airframe is modeled using linear normal modes data. Generalized masses, frequencies, and linear and angular mode shapes for 24 elastic modes are extracted by the finite element analysis program, NASTRAN. Figure 2 shows the CAMRAD II model for the medium utility helicopter.

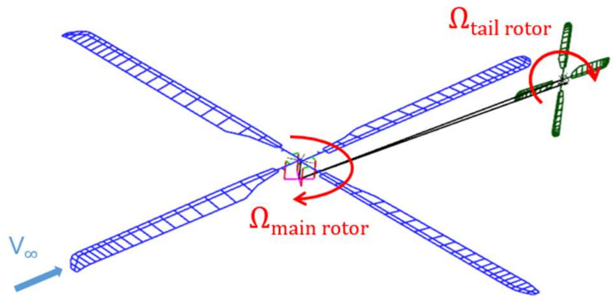

Figure 2: Geometry of CAMRAD II model.

2.2. Flight conditions and model validation

Level flights at 40 and 140 knots at 2,000 ft altitude under international standard atmospheric conditions are used for this study. This is because the target helicopter exhibits high vibration level at low- and high-speed flight conditions.

For the baseline model without the HHC application, the 4/rev vertical airframe vibrations at the airframe locations are calculated and validated against the flight test results at the cockpit (RH) and cabin (RH) locations shown in Figure 3.

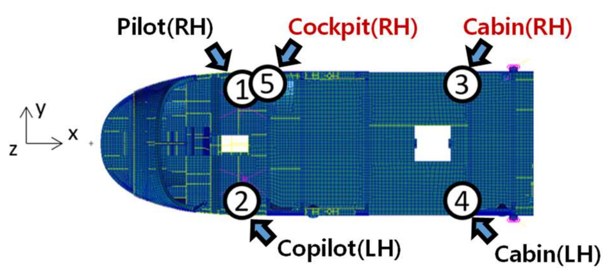

Figure 3: Vertical vibration calculation locations for validation.

The calculated vibration levels and the flight test data are compared in Figure 4. The magnitude of the acceleration has been normalized to the required vibration level in the fuselage. The average errors at 40 and 140 knots are 15.2% and 23.4% respectively. The calculation results do not agree exactly with the flight test results. However, as the relative magnitude of vibration by location and the relative change in vibration magnitude with changes in flight speed are well represented, it can be considered sufficient to predict the relative change in vibration due to the application of HHC in this study.

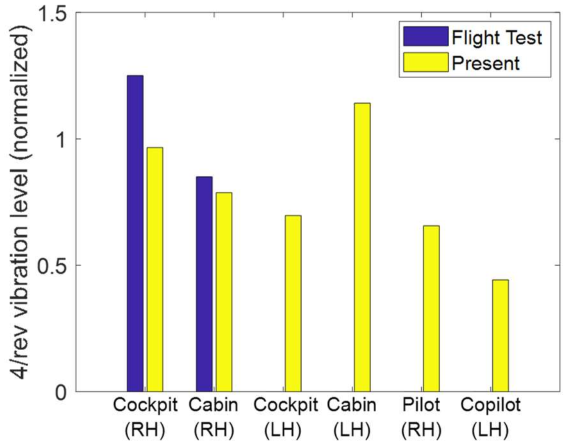

(a) 40 knots

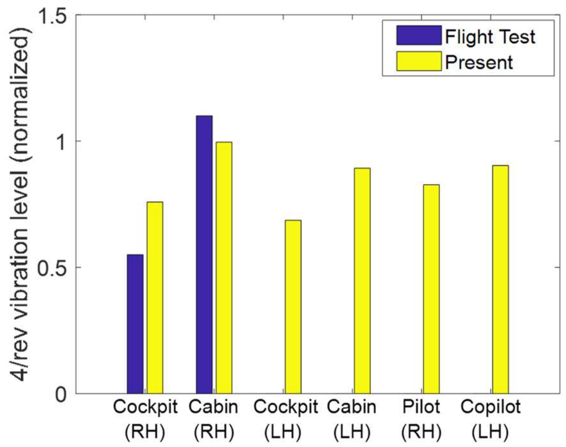

(b) 140 knots

Figure 4: Validations of 4/rev vertical vibration responses of the baseline model without HHC inputs.

3. HIGHER HARMONIC VIBRATION CONTROL SYSTEM

3.1. System architecture

Since the higher harmonic vibration control system is summarized in the authors' previous paper (Ref. 3), only the main points are briefly described in this paper. The architecture of the higher harmonic vibration control system is shown schematically in Figure 5. The HHC or multicyclic control system for vibration reduction is based on the linear, quasi-static, frequency domain model of the helicopter response (Refs. 4, 5). In steady state flight, the vibrations or loads on the helicopter are periodic, with a fundamental frequency of N_b/rev in the nonrotating frame. Harmonic analysis of the helicopter response is required to provide the harmonics of the vibrations or loads to the controller, and the higher harmonic control command is calculated by the controller and provided to the actuator. Finally, the actuators produce higher harmonic blade pitch angle changes.

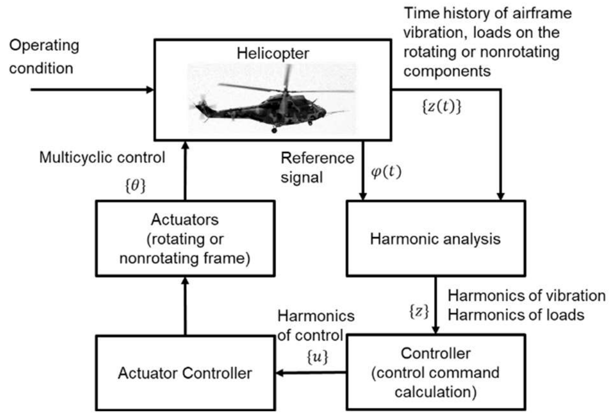

Figure 5: Architecture of the higher harmonic vibration control system.

The HHC actuators considered in this study are placed in nonrotating frame, therefore, m/rev (m = N_b, $2N_b$, …) control command can be applied in order to maintain the rotor track. Thus, the resulting m - 1, m, m + 1/rev components are generated in the blade pitch angles. For the simplification, the following simulations have been carried out only when m = N_b. When calculating steady-state flight using CAMRAD II, the higher harmonic components of the blade pitch angle can be input and the magnitude of the vibratory hub load or fuselage vibration can also be obtained in the form of harmonic components. By incorporating the changes in blade pitch angle induced by the HHC actuators, a linear system can be constructed which represents the correlation between the output of the vibratory hub load or fuselage vibration and the control input of the HHC actuators.

(1) $$z_n = z_0 + Tu_n$$

where, z is the output vector of the sine and cosine components of the N_b/rev harmonics of the vibration, and u is the input vector of the N_b/rev harmonics of the actuator control. T is the transfer function representing the helicopter model, and the subscript n represents the n-th step. In particular, z_0 represents the uncontrolled vibration response.

3.2. Vibratory hub load reduction

For vibratory hub load reduction, the response output vector z is defined as the N_b/rev components of the nonrotating hub forces, roll and pitch moments. Since N_b = 4 in this study, z is expressed as:

(2) $$z = \left[F_{x4C}\ F_{x4S}\ F_{y4C}\ F_{y4S}\ F_{z4C}\ F_{z4S}\ M_{x4C}\ M_{x4S}\ M_{y4C}\ M_{y4S}\right]^T$$

The control input vector u representing the N_b/rev motion of the three HHC actuators can be expressed as:

(3) $$u = [u_{1c} \quad u_{1s} \quad u_{2c} \quad u_{2s} \quad u_{3c} \quad u_{3s}]^T$$

The N_b/rev motion of the swashplate generated by the control input u can be calculated using the kinematic characteristics of the rotor system of the target helicopter. Then the blade pitch angle changes according to the swashplate motion can be calculated using the following relationship introduced in Ref. 6.

(4) $$\begin{Bmatrix} \theta_{(N_b-1)c} \\ \theta_{(N_b-1)s} \\ \theta_{N_bc} \\ \theta_{N_bs} \\ \theta_{(N_b+1)c} \\ \theta_{(N_b+1)s} \end{Bmatrix} = \begin{bmatrix} 0 & 1/2 & 0 & 0 & 1/2 & 0 \\ -1/2 & 0 & 0 & 0 & 0 & 1/2 \\ 0 & 0 & 1 & 0 & 0 & 0 \\ 0 & 0 & 0 & 1 & 0 & 0 \\ 0 & -1/2 & 0 & 0 & 1/2 & 0 \\ 1/2 & 0 & 0 & 0 & 0 & 1/2 \end{bmatrix} \begin{Bmatrix} S_{LNG,c} \\ S_{LNG,s} \\ S_{COL,c} \\ S_{COL,s} \\ S_{LAT,c} \\ S_{LAT,s} \end{Bmatrix}$$

where, θ is the blade pitch angle, S is the swashplate motion and the subscripts LNG, COL and LAT represent the longitudinal, collective and lateral motions respectively, and the subscripts C and S represent the cosine and sine components.

3.3. Airframe vibration reduction

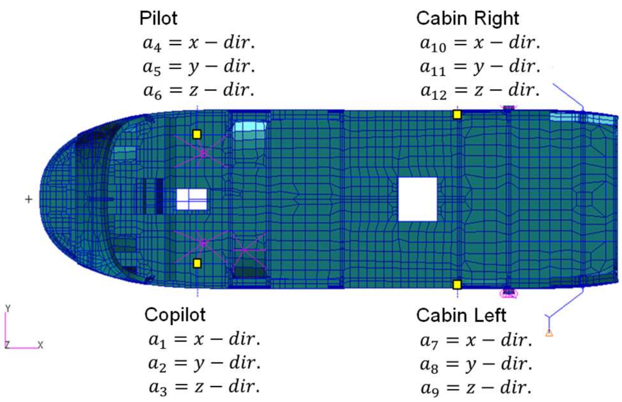

Figure 6: Locations of airframe acceleration sensors.

The same control input vector, eq. (3), is used for the airframe vibration reduction. But the response output vector, z, is the acceleration responses at four locations and three directions, i.e. the twelve accelerometer responses. The locations of the accelerometer are shown in Figure 6. These positions are different from those used for comparison with the flight test results in Figure 3, and have been selected with a view to the mounting locations in future tests.

(5) $$z = [a_{1c} \quad a_{1s} \quad a_{2c} \quad a_{2s} \quad \cdots \quad a_{12c} \quad a_{12s}]^T$$

where, a is the N_b/rev component of the acceleration, subscripts 1, 2, …, 12 are the number of accelerometers, and subscripts C and S are the cosine and sine components.

4. VIBRATORY HUB LOAD REDUCTION

The algorithm widely used in the higher harmonic vibration control system is optimal control, which minimizes the quadratic objective function. The general form of the quadratic performance function is:

(6) $$J = z_n^T W_z z_n + u_n^T W_u u_n + \Delta u_n^T W_{\Delta u} \Delta u_n$$

where, $\Delta u_n = u_n - u_{n-1}$, W_z is the weighting matrix for the response, W_u is the weighting matrix for the control input, and $W_{\Delta u}$ is the weighting matrix for the control rate. The control algorithm can be implemented in the form of open-loop control, closed-loop control, or adaptive control, and detailed formulations can be found in Refs. 4, 5 and 7.

4.1. System identification

The numerical system model $\hat{T}$ for the helicopter model T is calculated using the off-line system identification technique. A set of M test cases is used to obtain the transfer function model $\hat{T}$ using the following equation.

(7) $$\hat{T} = ZU^T(UU^T)^{-1}$$

where, Z is the response matrix containing M columns of the output z, and U is the input matrix containing M columns of control input u. The minimum number of the input-output data sets required for the system identification is equal to the number of independent control inputs, which is 6 for this study because there are 3 HHC actuators and 2 harmonic components, cosine and sine magnitudes. For a good estimation of the system model, more data sets must be used. Typically, two to three times the minimum number is recommended (Ref. 5). In this study, M = 36 is used, which is 6 times the minimum number of data sets. The 12 control inputs applied to each actuator are shown in Figure 7. The control input for each actuator was configured considering 50% and 100% amplitude and 6 phase angles as shown in Figure 7. The 100% amplitude was set based on the results of the authors' previous study (Ref. 3), which investigated the effectiveness of reducing vibratory hub load for the isolated rotor system model. The 100% amplitude of the HHC actuator corresponds to 2.43% of the full operating range of the MRA. The peak-to-peak amplitude, i.e. the full range over which the HHC actuator can move, is 4.86% of the MRA operating range. Therefore, the control authority of the HHC system is not large compared to the primary control system.

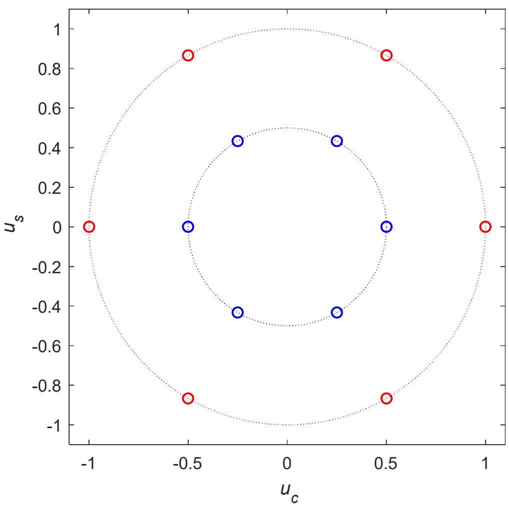

Figure 7: Control input for each actuator.

4.2. Optimal control input

To simplify the objective function to the sum of the squares of the vibratory loads, W_u and $W_{\Delta u}$ are set to zero. Then, the quadratic performance function, equation (6), is simplified as:

$$J = z_n^T W_z z_n \quad (8)$$

The output response weight matrix W_z is defined so that the objective function has a form similar to the vibration index (Ref. 2). The specified W_z is:

$$W_z = diag(\left(\tfrac{1}{2}\right)^2/W_0, \left(\tfrac{1}{2}\right)^2/W_0, \left(\tfrac{2}{3}\right)^2/W_0, \left(\tfrac{2}{3}\right)^2/W_0, 1/W_0, 1/W_0, 1/RW_0, 1/RW_0, 1/RW_0, 1/RW_0) \quad (9)$$

Then the performance function becomes:

$$J = \frac{(0.5F_{x,4})^2 + (0.67F_{y,4})^2 + (F_{z,4})^2}{W_0} + \frac{M_{x,4}{}^2 + M_{y,4}{}^2}{RW_0} \quad (10)$$

where, $(F_{x,4})^2 = (F_{x4C})^2 + (F_{x4S})^2$, R is the rotor radius, and W_0 is the operating weight of the target helicopter.

The optimal control input that minimize the performance function is obtained by:

$$u_{opt} = -(T^T W_z T)^{-1} T^T W_z z_0 \quad (11)$$

The optimal control inputs for the reduction of the vibratory hub load at 40 and 140 knots are shown in Figure 8. It can be seen that the optimal solutions calculated using the helicopter model are within the range of the actuator control authority selected by the isolated rotor model simulation results.

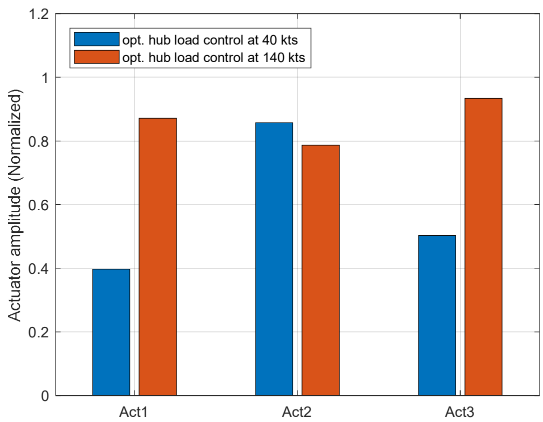

Figure 8: Optimal input for hub load reduction.

4.3. Vibratory hub load reduction performance

CAMRAD II calculation were performed using these optimum inputs and compared with the results of the linear system response calculations using the equation (1), as shown in Figure 9. Although the CAMRAD II calculation results show a larger F_z than the predicted F_z component at 140 knots, the overall response to the optimal control input is very close to the predicted results by the identified linear system.

5. AIRFRAME VIBRATION REDUCTION

5.1. System identification

The system identification was carried out in the same way as for the vibratory hub load reduction, using the same control input, but using equation (5) instead of equation (2) for the response output vector. The dimension of the identified helicopter model system is therefore 24 x 6.

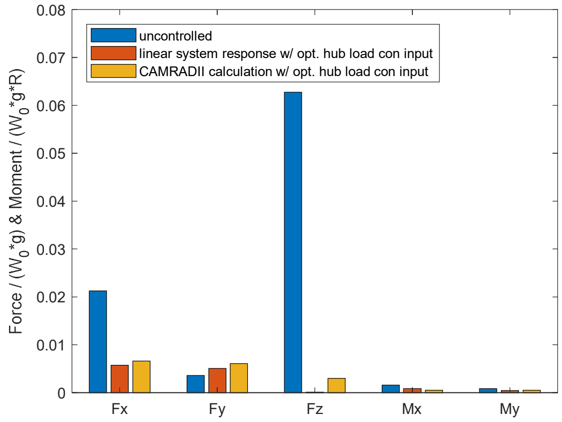

(a) 40 knots

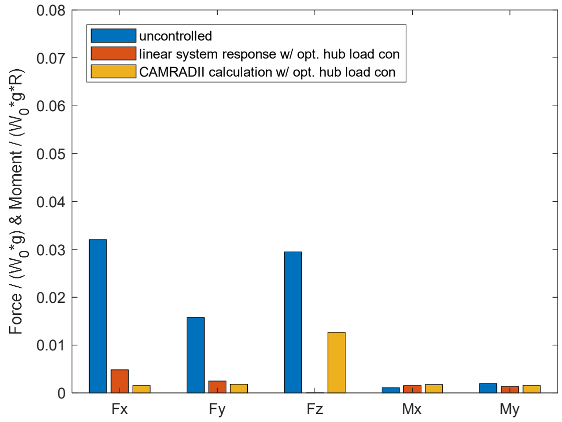

(b) 140 knots

Figure 9: Vibratory hub load responses to optimal control inputs.

5.2. Optimal control input

The optimal control input for airframe vibration reduction was calculated using the same quadratic performance function, equation (8). However, as the response output vector changed, the weight matrix was applied differently. Different weights can be applied to each accelerometer, but in this study, uniform weights were applied to all accelerometers.

(12) $$W_z = \mathrm{I}_{24\times 24}$$

The optimum control inputs for airframe vibration reduction at 40 and 140 knots are shown in Figure 10. It can be seen that the calculated optimum control input exceeds the predefined actuator amplitude. At low-speed flight, actuator 3 requires an amplitude of 180%, and at high-speed flight, actuator 2 requires an amplitude of 104%. Amplitude limitation can be applied in vibration control performance simulations, but only performance without actuator amplitude limitation was considered in this study.

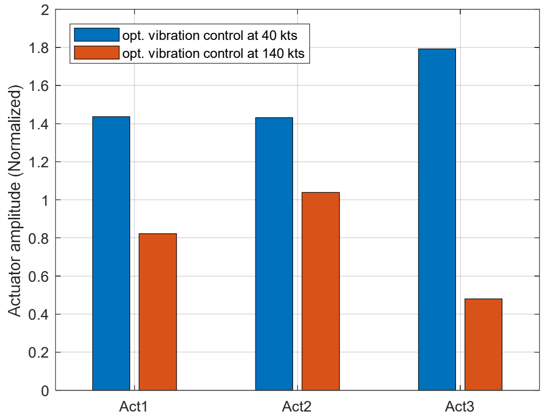

Figure 10: Optimal input for airframe vibration reduction.

5.3. Vibration reduction performance

The responses to the optimal control inputs are calculated using the equation (1) and compared with the CAMRAD II calculation results with the optimal control inputs. Figure 11 shows the magnitude of the uncontrolled vibration, the linear system response with optimal control and the results of the CAMRAD II calculations with optimal control inputs. The response of vertical accelerometers 3, 6, 9 and 12 is large when uncontrolled, but it can be seen that the vibration is greatly reduced when optimal control is applied. The CAMRAD II calculation results using the optimal control input show slight differences from the linear system response prediction results. This is because the identified linear system model does not perfectly simulate the actual helicopter model. As the non-linearity of the target helicopter system increases, the difference increases further.

Closed-loop control which minimizes the performance function by iteratively moving in the steepest descent direction, could be practical implementation method of higher harmonic vibration control system. The control command update equation of the gradient descent method is:

(13) $$u_{n+1} = u_n - \gamma T^T W_z z_n$$

where, $\gamma > 0$ is the step size or learning rate.

The system responses for different step sizes at 140 knots are shown in Figure 12. As γ increases, the convergence speed increases, but when it exceeds a certain value, the system diverges. When the step size value is chosen in a stable region, then the cost function converges to the optimal solution as the time step increases.

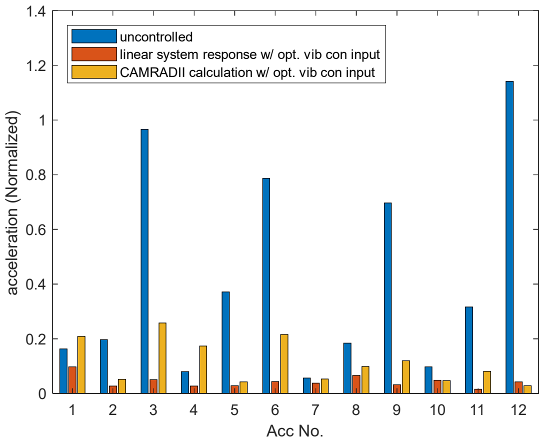

(a) 40 knots

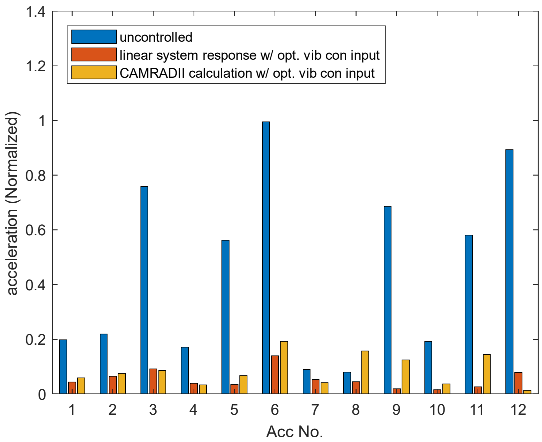

(b) 140 knots

Figure 11: Airframe vibration responses to optimal control inputs.

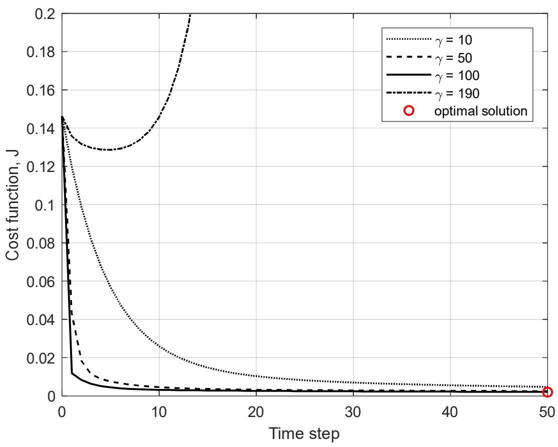

Figure 12: Closed-loop airframe vibration control performance at 140 knots as a function of step-size variations.

6. COMPARISON OF VIBRATORY HUB LOAD REDUCTION AND AIRFRAME VIBRATION REDUCTION

As can be seen in Figure 8 and Figure 10, it was observed that the optimum control input for vibratory hub load reduction and the optimum control input for airframe vibration reduction are different. This suggests that vibratory hub load reduction and airframe vibration reduction may not be achieved at the same time. Therefore, a comparative analysis of control inputs and vibration reduction performances is necessary.

6.1. Control input

The higher harmonic components of the blade pitch angles induced when the optimal control inputs are applied are shown in Figure 13. Overall, the 3/rev component contributes the most to the optimal solution, and the 5/rev component contributes the least. It can also be seen that the control input required to reduce airframe vibration is greatest at 40 knots.

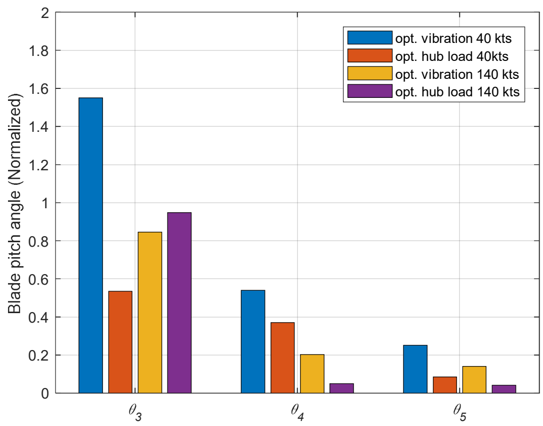

Figure 13: Harmonic components of the blade pitch angle at the optimum control inputs.

The higher harmonic blade pitch angle changes as a function of azimuth are shown in Figure 14. At 40 knots, the baseline waveforms of the higher harmonic blade pitch angles are the same at 3/rev, but the difference between the two optimal inputs is large. The amplitude of the optimal airframe vibration control is larger than the optimal vibratory hub load reduction input, and the difference between two control inputs becomes larger on the retreating side; the amplitude of the optimal vibratory hub load reduction on the retreating side is very small. On the other hand, at 140 knots, the two optimal control inputs are very close. There is a slight difference in the azimuth range of 320 ~ 50 degrees, but the overall waveforms are very close.

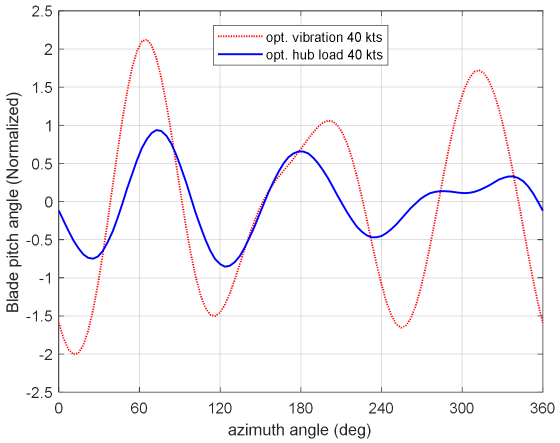

(a) 40 knots

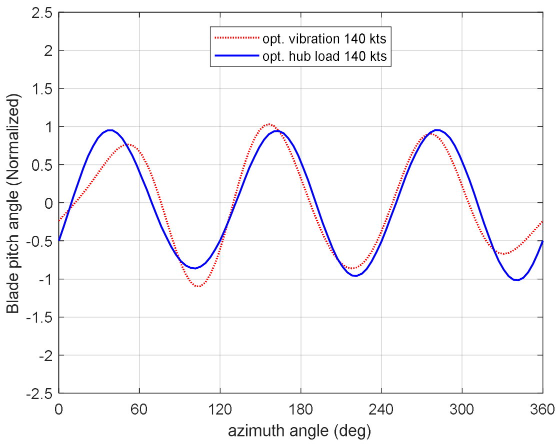

(b) 140 knots

Figure 14: Higher harmonic blade pitch angle changes produced by optimal control inputs

6.2. Vibratory hub load reduction performance

The vibratory hub load reduction performances when the two optimal control inputs are applied has been calculated using CAMRAD II and compared with the linear system responses in Figure 15.

Since the two control inputs are different at 40 knots and look similar at 140 knots, it is expected that the optimal control input for reducing airframe vibration is less effective in reducing vibratory hub load at 40 knots, while both control inputs are effective in reducing vibratory hub load at 140 knots. However, Figure 15 reveals that the response calculation results obtained from the linear system at both 40 knots and 140 knots indicate that the optimal control input for reducing airframe vibration has no effect on the reduction of vibratory hub load. At 140 knots, the control inputs in Figure 14 (b) are similar in appearance but are actually different. The CAMRAD II calculation results using the optimal airframe vibration control input show that there is a little reduction in the F_x and F_y, but the F_z is increased. Therefore, since the primary component of the vibratory hub load is F_z, it can be said that the optimal control input for reducing airframe vibration has no effect on the reduction of vibratory hub load.

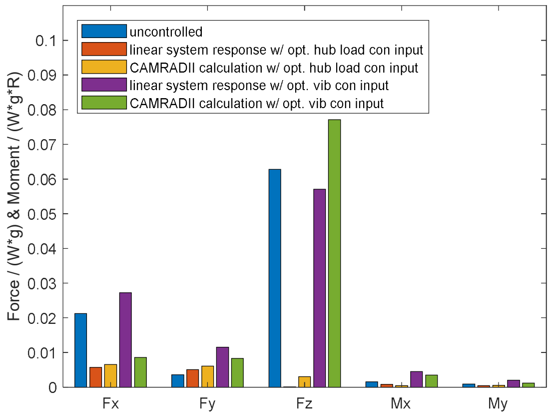

(a) 40 knots

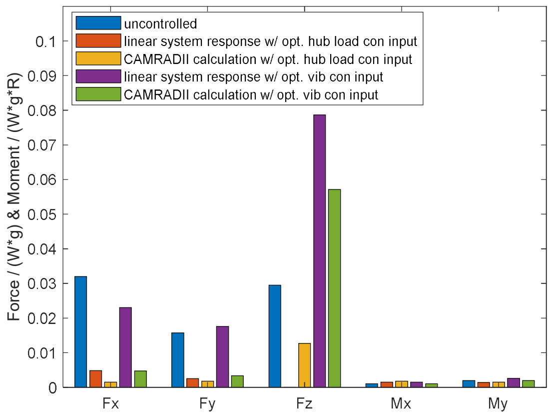

(b) 140 knots

Figure 15: Vibratory hub load responses to two different optimal control inputs.

When the optimal solution for vibratory hub load reduction is applied, the calculated vibratory hub load using the linear system model identified for hub load reduction are similar to the CAMRAD II calculation resut. However, the result calculated using the linear system identified for airframe vibration reducion is quite different from the CAMRAD II result.

6.3. Airframe vibration reduction performance

As in the preceding section, the airframe vibration reduction when the two optimal control inputs are applied has been calculated using CAMRAD II and compared with the linear system responses in Figure 16.

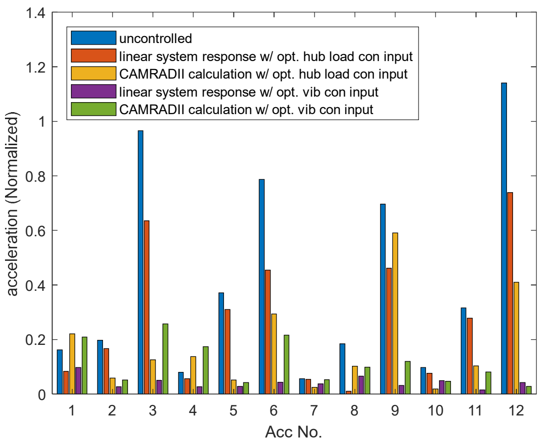

(a) 40 knots

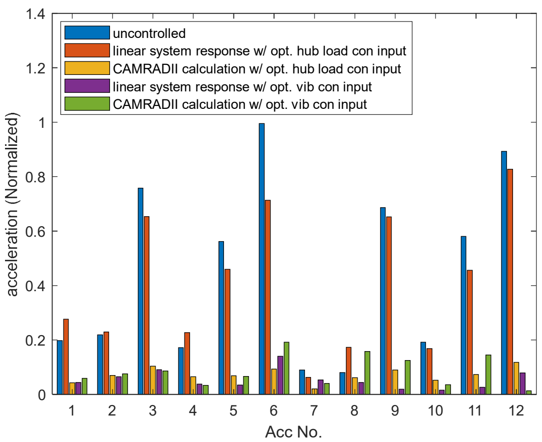

(b) 140 knots

Figure 16: Airframe vibration responses to two different optimal control inputs.

When employing the linear system model, the optimal control input for vibratory hub load reduction is found to have little impact on airframe vibration reduction at both low and high speeds. However, the CAMRAD II calculations indicate that the beneficial effect on airframe vibration reduction is achieved even when the control input for vibratory hub load reduction is utilized. At 40 knots, the CAMRAD II calculation results show that the vibration reduction performance at accelerometers 9 and 12 locations is somewhat poor when the optimal control input for vibratory hub load reduction is applied. However, the airframe vibration responses to the two optimal control inputs are very similar at 140 knots. In the case of vibratory hub load calculation using CAMRAD II at 140 knots, the F_z component responses to the two control inputs are observed to be significantly different. In contrast, in the case of airframe vibration prediction, the response at all accelerometer locations show good agreement. Here, the linear system is an approximation of the CAMRAD II calculation results, so the actual system response characteristics should be judged based on the CAMRAD II calculation result. Therefore, it can be said that the optimal control input for reducing vibratory hub load is also effective in reducing airframe vibration.

Similar to what was discussed in the previous section, the results of the airframe vibration calculation using the identified linear system model for vibratory hub load reduction are significantly different from the CAMRAD II results. The discrepancy in the system's response to the two optimal control inputs can be attributed to the fact that the two systems simulated as linear systems are different. First, the optimal solution provides a specific solution that minimizes the quadratic cost function, which varies depending on the uncontrolled response and the system matrix. And vibratory hub load reduction and airframe vibration reduction use different system matrices. Therefore, the two vibration control system models cannot predict the output of the other for the same control input. The differences between the CAMRAD II calculation results and the linear system responses can be explained by the fact that the linear system model is constructed by only one characteristic, vibratory hub load or airframe vibration, and there is an error due to linearization. If a linear system model is constructed that considers both vibratory hub load and airframe vibration, the prediction results using the linear system are expected to be more similar to the CAMRAD II calculation results.

7. CONCLUSIONS

The results of the vibration control simulations of the medium utility helicopter using the HHC system show that:

1. The vibratory hub load response calculated using the linear system that simulates the vibratory hub load and the optimal control input that minimizes it shows good agreement with the results

calculated using the CAMRAD II with this optimal control input.

2. The calculated airframe vibration using the linear system that simulates the airframe vibration and the optimal control input that minimizes it is similar to the calculated result by applying the same optimal control input to CAMRAD II.
3. The optimal control input for the airframe vibration reduction has no effect on the vibratory hub load reduction.
4. The optimal control input for reducing the vibratory hub load is also effective in reducing the airframe vibration.
5. The amplitude of the control input for reducing airframe vibration is larger than that for reducing vibratory hub load, especially at 40 knots.

In the future, vibration control simulations will be performed considering the actuator amplitude limitation. At that time, the vibratory hub load and the airframe vibration can be utilized as a response output to simultaneously reduce the vibratory hub load and the airframe vibration. Finally, the HHC actuator will be developed and tested on the aircraft.

Author contact:

Do-Hyung Kim dhkim@kari.re.kr

Jae-Sang Park aerotor@cnu.ac.kr

Dong-Gyue Kim ehdrb802@gmail.com

Woo-Ram Kang wooram.kang@koreaaero.com

8. ACKNOWLEDGMENTS

This work was supported by Korea Research Institute for defense Technology Planning and advancement (KRIT) grant funded by the Korea government (DAPA (Defense Acquisition Program Administration)) (No. KRIT-CT-21-020, Development of Higher Harmonic Control (HHC) SW for Helicopter Vibration Reduction, 2024).

9. REFERENCES

1. Kessler, C., “Active Rotor Control for Helicopters: Motivation and Survey on Higher Harmonic Control,” *CEAS Aeronautical Journal*, Vol. 1, (1–4), 2011, pp. 23–54.

2. van der Wall, B. G., Lim, J. W., Riemenschneider, J., Kallow, S., Wilke, G. A., Boyd, D. D. Jr., Bailly, J., Delrieux, Y., Cafarelli, I., Tanabe, Y., Sugawara, H., Jung, S. N., Hong, S. H., Kim, D.-H., Kang, H. J., Barakos, G., and Steininger, R., “Smart Twisting Active Rotor (STAR) – Pretest Predictions,” 48th European Rotorcraft Forum, Winterthur, Switzerland, 6-8 September 2022.

3. Kim, D.-H., Park, J.-S., and Bang, S.-W., “Feasibility and Effectiveness of a Higher Harmonic Control System for a Medium Utility Helicopter,” 49th European Rotorcraft Forum, Bückeburg, Germany, 5-7 September, 2023.

4. Johnson, W., “Self-Tuning Regulators for Multicyclic Control of Helicopter Vibration,” NASA TP 1996, 1982.

5. Chopra, I., and McCloud, J. L., III, “A numerical Simulation Study of Open-Loop, Closed-Loop, and Adaptive Multicyclic Control Systems,” *Journal of the American Helicopter Society*, Vol. 28, (1), Jan. 1983, pp. 63-77.

6. Biggers, J. C., and McCloud, J. L., III, “A Note on Multicyclic Control By Swashplate Oscillation,” NASA TM 78475, 1978.

7. Kim, D.-H., Hong, S., and Jung, S. N., “Multicyclic Vibration Control of a Helicopter Rotor with Active Twist Actuation,” *International Journal of Aeronautical and Space Sciences*, Vol. 23, No. 2, 2022, pp. 303-314. DOI: 10.1007/s42405-022-00440-z